Supplementary Information

Appendix A HBV Model

The HBV model is a commonly used rainfall-runoff model with routines for different components of the water cycle (e.g., snow routine, soil routine, groundwater routine for response and routing, etc.) [33, 74, 75]. The snow routine of the HBV model was used to capture (1) the partitioning of precipitation, $P(t)$ [L T^{-1}], between rainfall, $r(t)$ [L T^{-1}], and snowfall, and (2) the accumulation of snowpack and generation of snow melt, $s(t)$ [L T^{-1}]. Model parameters include (1) the threshold temperature, T_T [K], below which all precipitation is considered to fall as snow, (2) the snowfall correction factor, SF_{cf} [-], which accounts for snowfall undercatch due to wind turbulence, catchment vegetation, etc. [74, 76], (3) the degree-day factor, D_F [L T^{-1} K^{-1}], which is a proportionality constant for estimating snow melt, (4) the water holding capacity of the snowpack, W_H [-], and (5) the refreezing coefficient, F [-], which allows for refreezing of the melted water when air temperature, $T_{air}(t)$ [K], falls below T_T. Model parameters for snow accumulation were chosen to mimic weather conditions in the Mid-Atlantic U.S. (Table A1). To validate the HBV snow model results, we used data on daily accumulated snow depth at the nearby Dulles Airport (Figure A1), downloaded from the National Oceanic and Atmospheric Administration website

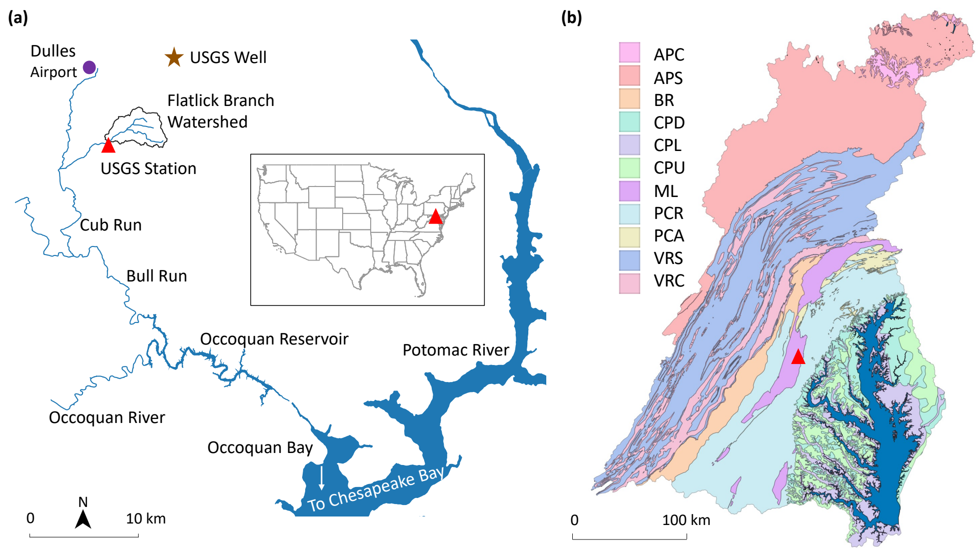

Fig. A1 (a) Flatlick Branch drains an urban watershed in Northern Virginia, and is tributary to the Occoquan Reservoir, where rising sodium concentrations threaten a critical water supply for up to 1 million people; (b) Flatlick Branch is located in the Mesozoic Lowland hydrogeomorphic (also referred to as the "Triassic Lowland") region of the Chesapeake Bay watershed (APC/APS: Appalachain Plateau Carbonate/Siliciclastic, BR: Blue Ridge, CPD/CPL/CPU: Coastal Plain Dissected Uplands/Lowlands/Uplands, ML: Mesozoic Lowlands, PCR/PCA: Piedmont Crystalline/Carbonate, VRS/VRC: Valley and Ridge Siliciclastic/Carbonate).

(www.ncei.noaa.gov), to verify that the timing of predicted snow melt events aligned with the date of zero accumulated snow depth reported at Dulles Airport after snow events. From these comparisons we estimated that the HBV snow model accurately predicts snow melt at Dulles roughly 83% of the time.

Table A1 HBV model parameters.

Parameter	Value
T_T	$0°$ C
SF_{cf}	1.1
D_F	7.29×10^{-5} m °C^{-1} h^{-1}
W_H	0.1
F	0.05

Appendix B Hydrologic Model

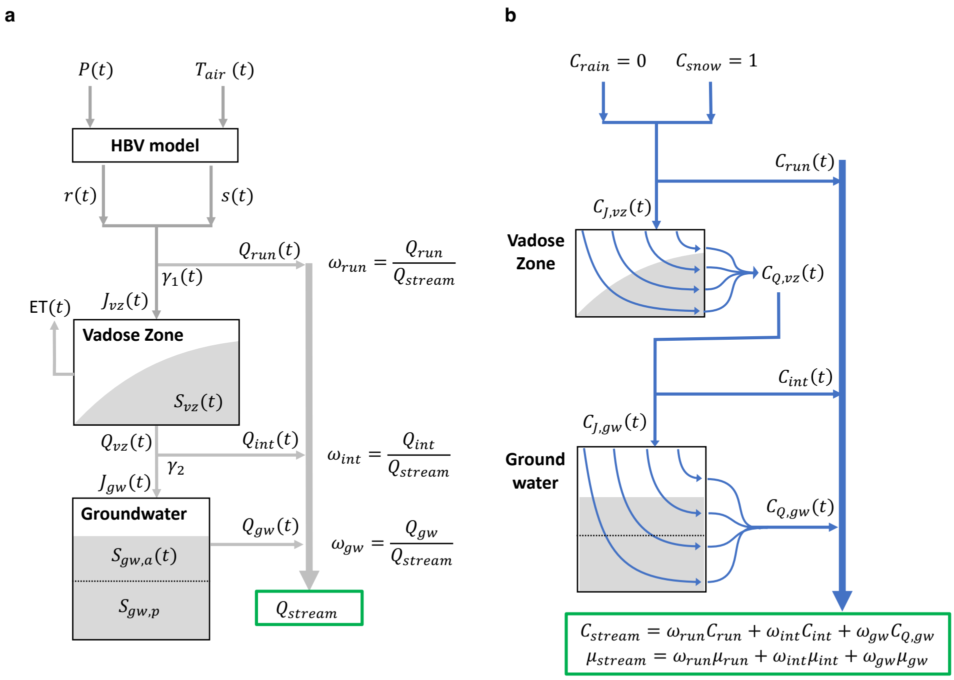

Fig. B2 Conceptual representation of the (a) hydrologic model and (b) transit time distribution model.

Stream flow was assumed to be the sum of direct runoff to the stream (e.g., through storm drain networks and overland flow), interflow through the vadose zone, and groundwater discharge: $Q_{\text{stream}}(t) = Q_{\text{run}}(t) + Q_{\text{int}}(t) + Q_{\text{gw}}(t)$ [L T^{-1}] (Figure B2a). The three terms on the right hand side of this equation were calculated as follows. A fraction, $\gamma_1(t)$ [-], of rain and snow melt (output from the HBV snow model) infiltrates to the vadose zone, $J_{\text{vz}}(t) = \gamma_1(t)(r(t) + s(t))$ [L T^{-1}], while the rest flows directly to the stream through storm drain networks and overland flow, $Q_{\text{run}}(t) = (1-\gamma_1(t))(r(t)+s(t))$ [L T^{-1}] (Vadose Zone storage, Figure 1a). Preliminary evaluation of the model indicated that infiltration into the vadose zone varies seasonally, presumably due to seasonal variations in vegetation cover and rainfall intensity (discussed further below) [77]. Accordingly, the infiltration fraction, $\gamma_1(t)$, was allowed to vary non-linearly with day, d, of the water year: $\log_{10}\gamma_1(t) = x + i \sin \frac{2\pi(d+p)}{365}$. In this expression, $d = 0$ corresponds to the beginning of the water year, October 1st, and the parameters x [-], i [-], and p set, respectively, the annual average infiltration, magnitude of the seasonal signal, and phase of the seasonal signal. For the top model (with the lowest RMSE, see Table 1), the set of values inferred for x, i, and p suggest that the fraction of inflow that enters the vadose zone through infiltration is higher in the winter and lower in the summer.

We hypothesized that most of this seasonality arises from seasonal variations in the intensity of storm events; specifically, if summer storms are frequently more intense than winter storms, a larger fraction of summer-time rainfall would enter the stream as direct runoff, and a smaller fraction would enter the vadose zone through infiltration. An analysis of output from the HBV snow model (i.e., hourly estimates of inflow to the catchment from either rainfall or snow melt) supports this hypothesis. From the HBV snow model, we obtained ten years of hourly estimates for inflow to the catchment from either rainfall or snow melt (N=87672). We started our analysis by removing from this timeseries all instances where the HBV snow model predicted zero inflow (i.e., we removed all dry weather periods). From the remaining non-zero inflow intensity values (N=7250) we constructed three probability distributions, one for inflow during the summer (June, July and August), one for inflow during the winter (December, January, February), and one for inflow year round. Consistent with our hypothesis, the distributions for winter and summer inflow intensities peak around 0.2 and 0.5 mm h^{-1}, respectively, and very intense storms (up to 6 mm h^{-1}) are more frequent in the summer (Figure B3). The seasonal difference in inflow intensities can also be documented by examining the raw data. Over the ten year time period, the number of hours when summer and winter inflow intensities exceeded 2 mm h^{-1} were N=320 and 253, respectively. Conversely, the number of hours when summer and winter inflow intensities were below 2 mm h^{-1} were N=685 and 2479, respectively. Thus, lower intensity inflow events are more frequent in the winter than the summer, while higher intensity inflow events are more frequent in the summer than the winter. This analysis supports our hypothesis that the most of the seasonal variation in $\gamma_1(t)$ reflects runoff generation during intense summer rains.

Once water enters the vadose zone, $J_{\text{vz}}(t)$ [L T^{-1}], it can accumulate with time, $\frac{dS_{\text{vz}}}{dt}$ [L T^{-1}], leave by evapotranspiration, ET(t) [L T^{-1}], or leave by discharge, $Q_{\text{vz}}(t)$ [L T^{-1}]: $\frac{dS_{\text{vz}}}{dt} = J_{\text{vz}}(t) - Q_{\text{vz}}(t) - ET(t)$. Reflecting the influence of capillary forces

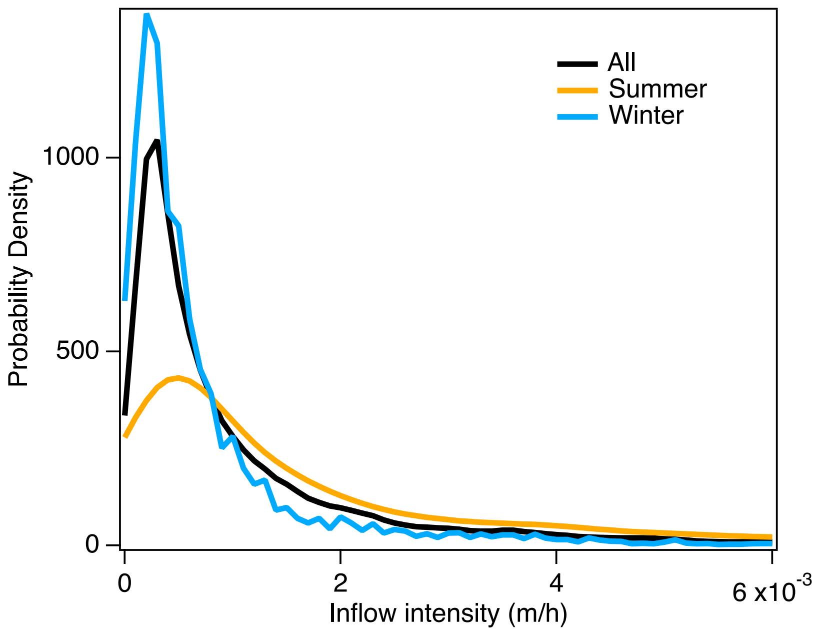

Fig. B3 Probability distributions for inflow intensities for summer (June, July, August), winter (December, January, February) and all days of the study period.During summer, probability for high intensity ($> 2 \times 10^{-3}$ m/h) inflows is greater (yellow curve) than during winter (blue curve), suggesting higher runoff generation (and consequently lower infiltration) during summer months.

on transiently saturated flow, the discharge-storage relationship for the vadose zone is presumed to be non-linear [66, 78]: $Q_{\mathrm{vz}}(t) = K_{\mathrm{sat}}\left(\frac{S_{\mathrm{vz}}(t)}{S_{\mathrm{vz,max}}}\right)^{g}$, where K_{sat} [L T^{-1}], $S_{\mathrm{vz,max}}$ [L] and g [-] represent, respectively, the saturated hydraulic conductivity of the vadose zone, maximum depth of the vadose zone, and a power-law exponent. Evapotranspiration was calculated from the product of vadose zone saturation and hourly estimates of potential evapotranspiration, PET(t) [L T^{-1}], obtained from the NASA Land Surface Model [78]: $\mathrm{ET}(t) = \frac{S_{\mathrm{vz}}(t)}{S_{\mathrm{vz,max}}}\mathrm{PET}(t)$. A fixed fraction γ_2 of outflow from the vadose zone infiltrates to groundwater, $J_{\mathrm{gw}}(t) = \gamma_2 Q_{\mathrm{vz}}(t)$ [L T^{-1}], while the rest flows to the stream as interflow, $Q_{\mathrm{int}}(t) = (1-\gamma_2)Q_{\mathrm{vz}}(t)$ [L T^{-1}].

Water entering groundwater, $J_{\mathrm{gw}}(t)$ [L T^{-1}] can accumulate with time, $\frac{dS_{\mathrm{gw}}}{dt}$ [L T^{-1}], or flow to the stream, $Q_{\mathrm{gw}}(t)$ [L T^{-1}]: $\frac{dS_{\mathrm{gw}}}{dt} = J_{\mathrm{gw}}(t) - Q_{\mathrm{gw}}(t)$. Groundwater storage is divided into an active portion that influences stream flow, $S_{\mathrm{gw,a}}(t)$ [L], and a fixed passive portion, $S_{\mathrm{gw,p}}$ [L], that does not influence stream flow but can store and release solutes [18]: $S_{\mathrm{gw}}(t) = S_{\mathrm{gw,a}}(t) + S_{\mathrm{gw,p}}$. The groundwater discharge-storage relationship depends linearly on active storage [79]: $Q_{\mathrm{gw}}(t) = k_{\mathrm{gw}} S_{\mathrm{gw,a}}(t)$ where k_{gw} [T^{-1}] is a response rate constant for the active portion of groundwater storage. The coupled set of differential equations for storage in the vadose zone and groundwater were numerically integrated within Wolfram Mathematica (v. 12.3).

Appendix C Transient-Transit Time Distribution (T-TTD) Model

T-TTD theory was used to estimate, on an hourly basis, the mean age of water in the stream and the fraction of stream flow derived originally from snow melt, assuming that outflow from the vadose zone and groundwater is selected uniformly by age; i.e., a uniform storage selection function was adopted for both the vadose zone and groundwater control volumes (Figure B2) [35, 80]. These calculations are described in turn.

C.1 Deriving Solutions for the Mean Age of Water

The mean age of water in the stream, $\mu_{\mathrm{stream}}(t)$ [T], was calculated from the expected value of the stream's age distribution, $\mu_{\mathrm{stream}}(t) = \int_0^\infty T p_{\mathrm{stream}}(T,t)dT$, where the variable T represents water age and $p_{\mathrm{stream}}(T,t)$ [T^{-1}] is the probability density function (PDF) form of the stream's age distribution at any time t. The latter can be expressed as the flow-weighted sum of age distributions in runoff, interflow and groundwater discharged to the stream: $p_{\mathrm{stream}}(T,t) = \omega_{\mathrm{run}}(t)p_{\mathrm{run}}(T,t) + \omega_{\mathrm{int}}(t)p_{\mathrm{int}}(T,t) + \omega_{\mathrm{gw}}(t)p_{\mathrm{gw}}(T,t)$. The weighting functions are defined as follows:

$$\omega_{\mathrm{run}}(t) = \frac{Q_{\mathrm{run}}(t)}{Q_{\mathrm{stream}}(t)},\ \omega_{\mathrm{int}}(t) = \frac{Q_{\mathrm{int}}(t)}{Q_{\mathrm{stream}}(t)},\ \omega_{\mathrm{gw}}(t) = \frac{Q_{\mathrm{gw}}(t)}{Q_{\mathrm{stream}}(t)}, \tag{C1}$$

Combining these equations we arrive at the following expression for the mean age of water in the stream at any time t, where $\mu_{\mathrm{run}}(t)$, $\mu_{\mathrm{int}}(t)$, and $\mu_{\mathrm{gw}}(t)$ are the expected values of water age in direct runoff, interflow and groundwater, respectively:

$$\mu_{\mathrm{stream}}(t) = \omega_{\mathrm{run}}(t)\mu_{\mathrm{run}}(t) + \omega_{\mathrm{int}}(t)\mu_{\mathrm{int}}(t) + \omega_{\mathrm{gw}}(t)\mu_{\mathrm{gw}}(t) \tag{C2}$$

For this analysis we assumed that runoff has a single age, T_{run} [T], when it is reaches the stream: $p_{\mathrm{run}}(T,t) = \delta(T - T_{\mathrm{run}})$, where δ is the Dirac Delta function. Therefore, the mean age of runoff entering the stream is $\mu_{\mathrm{run}}(t) = T_{\mathrm{run}}$.

The formulae used to estimate the mean age of water in interflow and groundwater were derived by first constructing a generic solution for the mean age of water leaving a control volume assuming that: (1) inflow has some prescribed age distribution which can vary with time; (2) outflow from the control volume occurs by both discharge and evapotranspiration; and (3) water leaving the control volume by discharge and evapotranspiration is sampled from storage uniformly by age. This generic solution for the mean age of water in, and leaving, a control volume was then tailored to yield separate formulae for the mean age of water entering the stream from the vadose zone and groundwater.

C.2 Mean Age of Water Leaving a Generic Control Volume

Consider a control volume drawn around either the vadose zone or groundwater (see below) that receives inflow at rate, $J(t)$ [L T^{-1}], and loses water through discharge at rate, $Q(t)$ [L T^{-1}], and evapotranspiration at rate, $ET(t)$ [L T^{-1}] (all volumes and fluxes are normalized by the catchment area). From volume balance, the change in water stored in the control volume, $S(t)$ [L], is therefore equal to the instantaneous difference between inflows and outflows: $\frac{dS}{dt} = J(t) - Q(t) - ET(t)$. We make the following additional assumptions: (1) water entering the control volume with inflow $J(t)$ has an age distribution that varies with time, $P_{in}(T, t)$ [-], where the variable T represents the random variable for water age, and the age distribution is expressed as a cumulative distribution function (CDF); and (2) water leaving the control volume by either discharge $Q(t)$ or evapotranspiration $ET(t)$ is uniformly sampled from water in storage (i.e., a uniform StorAge Selection (SAS) function is adopted for both discharge and evapotranspiration). Under such conditions, the time evolution of the age distribution of water stored in the control volume, $P(T, t)$ [-], expressed here as a CDF, is governed by the following Age Conservation Equation (ACE) [37]:

$$\frac{\partial S(t)P(T,t)}{\partial t} = J(t)P_{in}(T,t) - ET(t)P(T,t) - Q(t)P(T,t) - S(t)\frac{\partial P(T,t)}{\partial T} \quad \text{(C3a)}$$

$$P(T = 0, t) = 0 \quad \text{(C3b)}$$

$$P(T, t = 0) = H(T - T_0) \quad \text{(C3c)}$$

$$H(x) = \begin{cases} 0, x < 0 \\ 1, x \geq 0 \end{cases} \quad \text{(C3d)}$$

In this equation, the time rate of change in the fraction of water in storage with age less than or equal to T (left hand side) depends on the inflow of water of age $P_{in}(T, t)$ (first term on right hand side), outflow of water by evapotranspiration and discharge under uniform selection (second and third terms), and the aging of water in storage with time (fourth term). The boundary condition (Equation C3b) stipulates that there is no water in storage with age less than or equal to $T = 0$, while the initial condition (Equation C3c) stipulates that water in storage at time $t = 0$ has a single age equal to $T = T_0$, where $H(\cdot)$ is the unit step or Heaviside function (Equation C3d). Expanding the left hand side of the equation and substituting the conservation equation for water in storage we obtain the following simplified form of the ACE:

$$S(t)\frac{\partial P(T,t)}{\partial t} = J(t)(P_{in}(T,t) - P(T,t)) - S(t)\frac{\partial P(T,t)}{\partial T} \quad \text{(C4)}$$

The ACE can also be expressed in terms of probability density functions (PDFs) for the age distributions of water leaving and entering the control volume ($p(T, t)$ and $p_{in}(T, t)$, respectively), by taking the derivative of both sides of Equation C4 with respect to the age variable T, where $p(T, t) = \frac{\partial P(T,t)}{\partial T}$ and $p_{in}(T, t) = \frac{\partial P_{in}(T,t)}{\partial T}$:

$$S(t)\frac{\partial p(T,t)}{\partial t} = J(t)(p_{in}(T,t) - p(T,t)) - S(t)\frac{\partial p(T,t)}{\partial T} \quad \text{(C5a)}$$

$$p(T = 0, t) = 0 \quad \text{(C5b)}$$

$$p(T, t = 0) = \delta(T - T_0) \quad \text{(C5c)}$$

The PDF form of the boundary and initial conditions (Equations C5b and C5c), follows by differentiating Equations C3b and C3c with respect to the age variable T. Taking the expected value, $\int_0^\infty T\,(\cdot)\,dT$, of each term in the PDF form of the ACE along with its boundary and initial conditions (Equations C5a-C5c) yields, after some manipulation, the following differential equation for the mean age of water in storage:

$$\frac{d\mu(t)}{dt} = \frac{J(t)}{S(t)}(\mu_{in}(t) - \mu(t)) + 1, \ S(t) > 0 \tag{C6a}$$

$$\mu(t = 0) = T_0 \tag{C6b}$$

Here, $\mu(t)$ represents the mean age (or expected value) of the water in and leaving the control volume at any time t, and $\mu_{in}(t)$ represents the mean age (or expected value) of water entering the control volume with inflow at any time t: $\mu(t) = \int_0^\infty Tp(T,t)dT$ and $\mu_{in}(t) = \int_0^\infty Tp_{in}(T,t)dT$. The above differential equation can be solved to yield the following exact solution for the mean age of water discharged from the control volume under uniform sampling:

$$\mu(t) = T_0 e^{-\tau_{\mathrm{J}}(t)} + \int_0^t e^{-(\tau_{\mathrm{J}}(t) - \tau_{\mathrm{J}}(x))}\left(1 + \frac{J(x)}{S(x)}\mu_{in}(x)\right)\,dx, \ S(t) > 0 \tag{C7a}$$

$$\tau_{\mathrm{J}}(t) = \int_0^t \frac{J(\nu)}{S(\nu)}d\nu \tag{C7b}$$

In the event that the water coming into the tank has a mean age of $\mu_{in} = 0$, the above solution simplifies as follows:

$$\mu(t) = T_0 e^{-\tau_{\mathrm{J}}(t)} + \int_0^t e^{-(\tau_{\mathrm{J}}(t) - \tau_{\mathrm{J}}(x))}\,dx, \ \mu_{in}(t) = 0, \ S(t) > 0 \tag{C8a}$$

C.3 Mean Age of Water in Interflow

From the generic solution presented above, the mean age of water leaving the vadose zone and entering the stream as interflow can be written as follows, where we have assumed the initial age of water in the vadoze zone at time $t = 0$ is, $T_{0,vz} = 0$:

$$\mu_{int}(t) = \int_0^t e^{-(\tau_{\mathrm{J,vz}}(t) - \tau_{\mathrm{J,vz}}(x))}\,dx, \ S_{vz}(t) > 0 \tag{C9a}$$

$$\tau_{\mathrm{J,vz}}(t) = \int_0^t \frac{J_{vz}(\nu)}{S_{vz}(\nu)}d\nu \tag{C9b}$$

C.4 Mean Age of Water in Groundwater

Accounting for the fact that water entering the groundwater (from the vadose zone) has some time varying mean age, $\mu_{int}(t)$, and building on the results presented above, we can write down the following solution for the mean age of water leaving the groundwater and entering the stream:

$$\mu_{gw}(t) = T_{0,gw} e^{-\tau_{\mathrm{J,gw}}(t)} + \int_0^t e^{-(\tau_{\mathrm{J,gw}}(t) - \tau_{\mathrm{J,gw}}(x))} \left(1 + \frac{J_{gw}(x)}{S_{gw,a}(x) + S_{gw,p}} \mu_{int}(x)\right) dx, \;\; S_{gw}(t) > 0 \tag{C10a}$$

$$\tau_{\mathrm{J,gw}}(t) = \int_0^t \frac{J_{gw}(\nu)}{S_{gw,a}(\nu) + S_{gw,p}} d\nu \tag{C10b}$$

Implementation of this last solution requires that we specify a value for the passive groundwater depth, $S_{gw,p}$. All else being equal, the model-predicted mean age of groundwater will increase as the depth of the passive groundwater is increased. Subsurface flow discharged to streams in the Mesozoic Lowland hydrogeomorphic region (HGMR, where Flatlick Branch is located, see Figure A1b) is much younger than that in other Chesapeake Bay HGMRs (Figure C4). For the Flatlick Branch catchment, the median age of subsurface flow discharged to stream is 5.2 years [38] (right panel in Figure C4).

To identify the passive groundwater depth that would yield a similar model-predicted median subsurface flow age, we conducted the following numerical experiment. First, to provide sufficient time for the mean age of groundwater to reach a dynamic equilibrium, we created a 30-year synthetic time series of hourly precipitation, temperature and PET (the inputs to our HBV and Hydrologic models), by repeating the measured ten-year hourly time series for these three climate variables at our site a total of three times. Second, using the parameter values for the top-ranked model (see Table 1) we solved the HBV and Hydrologic models (see Sections A and B) for the entire 30-year period, yielding hourly estimates for all stocks and flows of water through the catchment. Third, from the 30-year time series of catchment stocks and flows we computed hourly estimates for the mean ages of water discharged to the stream from the vadose zone and groundwater (from equations (C9a) and (C10a), respectively). This allowed us to calculate the mean age of subsurface flow using the following equation:

$$\mu_{\mathrm{sub}}(t) = \frac{Q_{\mathrm{int}}(t)}{Q_{\mathrm{int}}(t) + Q_{\mathrm{gw}}(t)} \mu_{\mathrm{int}}(t) + \frac{Q_{\mathrm{gw}}(t)}{Q_{\mathrm{int}}(t) + Q_{\mathrm{gw}}(t)} \mu_{\mathrm{gw}}(t) \tag{C11}$$

Finally, we computed the median subsurface flow age from the last six years of hourly mean subsurface flow age simulations. The last two steps were then repeated for 5 different choices of the passive groundwater depth, ranging from 0 to 1.5 m. The results of this numerical experiment, which are presented in Figure C5, indicate that the median groundwater age increases linearly with passive groundwater storage.

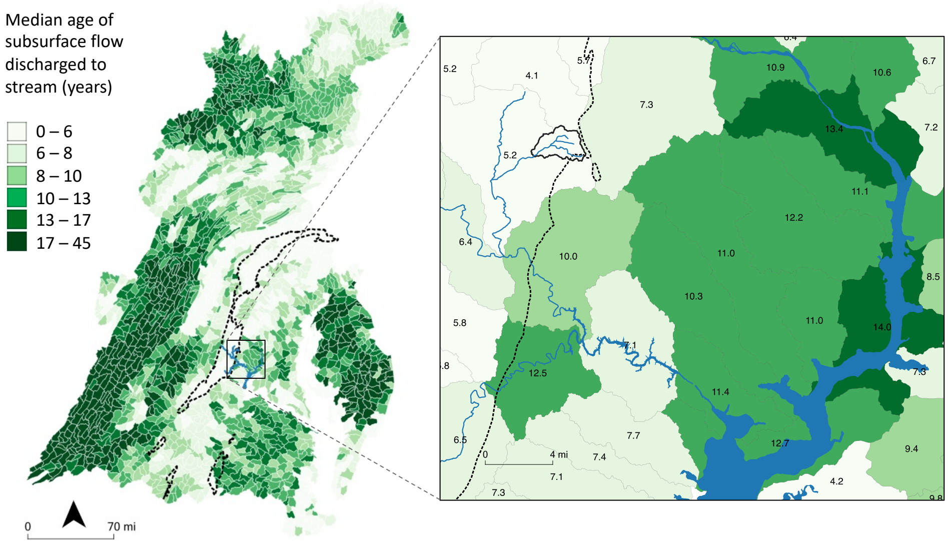

Fig. C4 Median age of subsurface flow discharged to streams in different sub-watersheds within the Chesapeake Bay watershed. Thick dashed curve denotes the Mesozoic Lowland HGMR. Solid black line (right panel) denotes the Flatlick Branch catchment.

From this plot we infer that, for the Flatlick Branch site, a median subsurface flow age of 5.2 years corresponds to a passive groundwater depth of $S_{gw,p} \approx 1.4$m. This choice of passive groundwater depth was therefore adopted for all age simulations described in the main text. We also adopted $T_{0,vz} = 0$ years and $T_{0,gw} = 15$ years for the initial ages of water in the vadose zone and groundwater, respectively.

C.5 Snow Melt Fraction

In Figure B2b, the variable, $C_{\text{stream}}(t) \in [0, 1]$ [-], represents the fraction of stream flow, at any time t, that originated as snow melt. The end members, $C_{\text{stream}}(t) = 1$ or $C_{\text{stream}}(t) = 0$, therefore represent conditions where the stream flow is 100% derived from snow melt or rainfall, respectively. As noted in the main text, we assumed that direct runoff has an effective age of $T_{run} = 0$. Given this assumption and for the choice of a uniform StorAge Selection (SAS) function for discharge from the vadose zone and groundwater (*45*), the fraction $C_{\text{stream}}(t)$ can be estimated directly from solute mass balance and the dynamic water balance calculations presented in Section B, as the flow weighted sum of the snow melt fraction of runoff, interflow, and groundwater ($C_{\text{run}}(t)$, $C_{\text{int}}(t)$, $C_{\text{gw}}(t)$, respectively):

$$C_{\text{stream}}(t) = \omega_{\text{run}}(t)C_{\text{run}}(t) + \omega_{\text{int}}(t)C_{\text{int}}(t) + \omega_{\text{gw}}(t)C_{\text{gw}}(t) \tag{C12a}$$

$$C_{\text{run}}(t) = C_{J,vz}(t) = \frac{s(t)}{s(t) + r(t)} \tag{C12b}$$

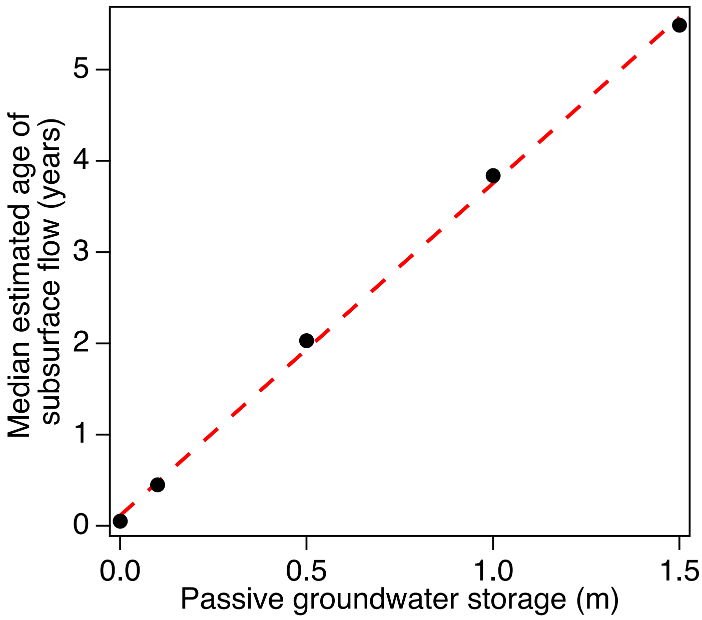

Fig. C5 Model-predicted median subsurface flow age discharged to Flatlick Branch for different choices of passive groundwater storage depth.

$$C_{\mathrm{int}}(t) = C_{J,gw}(t) = \frac{1}{S_{\mathrm{vz}}(t)} \int_0^t C_{J,vz}(t_i) J_{vz}(t_i) e^{-(\tau_{\mathrm{Q,vz}}(t) - \tau_{\mathrm{Q,vz}}(t_i))}\, dt_i \tag{C12c}$$

$$C_{\mathrm{gw}}(t) = \frac{1}{S_{\mathrm{gw,a}}(t) + S_{\mathrm{gw,p}}} \int_0^t C_{J,gw}(t_i) J_{gw}(t_i) e^{-(\tau_{\mathrm{Q,gw}}(t) - \tau_{\mathrm{Q,gw}}(t_i))}\, dt_i \tag{C12d}$$

$$\tau_{\mathrm{Q,vz}}(t) = \int_0^t \frac{Q_{\mathrm{vz}}(r) + \mathrm{ET}(r)}{S_{\mathrm{vz}}(r)} dr \tag{C12e}$$

$$\tau_{\mathrm{Q,gw}}(t) = \int_0^t \frac{Q_{\mathrm{gw}}(r)}{S_{\mathrm{gw,a}}(r) + S_{\mathrm{gw,p}}} dr \tag{C12f}$$

The expression for $C_{\mathrm{run}}(t)$ follows from a mass balance over rainfall and snow melt entering the catchment with snow melt fractions of $C_{rain} = 0$ and $C_{snow} = 1$, respectively (Equation C12b and top of Figure B2b). The integrals appearing in Equations C12c and C12d represent the sum over all snow melt entering the vadose zone and groundwater control volumes, respectively, from time $t_i \in [0, t]$. The exponential terms appearing in these integrals account for the outflow of snow melt under uniform sampling, the rate of which depends on outflow-weighted time $\tau_{\mathrm{Q}}(t)$ [-]. The latter takes on different functional forms for the vadose zone (where snow melt can leave the control volume by both discharge and evapotranspiration, Equation C12e) and groundwater (where snow melt leaves the control volume by discharge alone, Equation C12f). As described above, for these calculations we set the volume of passive groundwater to $S_{\mathrm{gw,p}} = 1.4$m.

Appendix D Model Calibration

D.1 Data Sources

HBV and hydrologic model predictions of catchment hydrology are driven by hourly measurements of precipitation, air temperature, and potential evapotranspiration (PET) (Figure B2a and Figure 1a). Ten years (water years 2008-2017) of measured hourly precipitation (with a heated gage) and air temperature at Dulles International Airport (station ID WBAN:93738, located approximately 6 km north of the Flatlick monitoring station, see Figure A1a) were downloaded from the National Oceanic and Atmospheric Administration website (www.ncei.noaa.gov). Hourly estimates of local PET (for a pixel ($0.125° \times 0.125°$) centered on the nearby Occoquan Forest) were obtained from NASA's land surface model (NLDAS-Noah) using the Data Rods Explorer (apps.hydroshare.org/apps/data-rods-explorer). Daily groundwater elevation (in feet to groundwater from land surface, for comparison with model-predictions of active groundwater depth, see Figure J10) were obtained for USGS well (#385638077220101), located approximately 10 km northeast of the USGS stream monitoring station on Flatlick Branch (Figure A1). The hydrologic model was calibrated and validated with ten-years (water years 2008-2017) of hourly stream flow measurements at a USGS monitoring station on Flatlick Branch (USGS Station ID 01656903 Figure A1). T-TTD predictions of mean stream water age and snow melt fraction (Section C) were compared with hourly in situ measurements of specific conductance, which was collected at the same location on Flatlick Branch (USGS Station ID 01656903), and over the same ten-year time period (water years 2008-2017) as the stream flow measurements described above.

D.2 Parameter Inference

The hydrological component of our modeling framework includes seven parameters, which were inferred from stream flow measurements at Flatlick Branch as described in Section 13. Preliminary evaluation indicated that the posterior distributions of all parameters were well constrained (see Figures 1 c,d), with the exception of the active groundwater response rate for which the posterior values were more uniformly distributed, a problem also noted by Bertuzzo et al. [79]. As noted in the main text, we fixed the active groundwater response rate to $k_{\mathrm{gw}} = 0.11$ day^{-1}, based on the slope of log-transformed measurements of stream flow at Flatlick Branch against time for the master recession curve (Figure D6). Posterior distributions were derived for the remaining six parameters conditioned on this single value for the active groundwater response rate.

Appendix E Estimating Deicer Application Rates

In Northern Virginia, winter maintenance responsibilities fall under the jurisdiction of both public sector agencies (e.g., on roads, parking lots, etc.) and private sector companies (e.g., on private properties) [64]. Virginia Department of Transportation (VDOT) guidelines for deicer application rates in this area (which are based on Salt Institute's standard road salt (as NaCl) application rates) are keyed to winter-weather

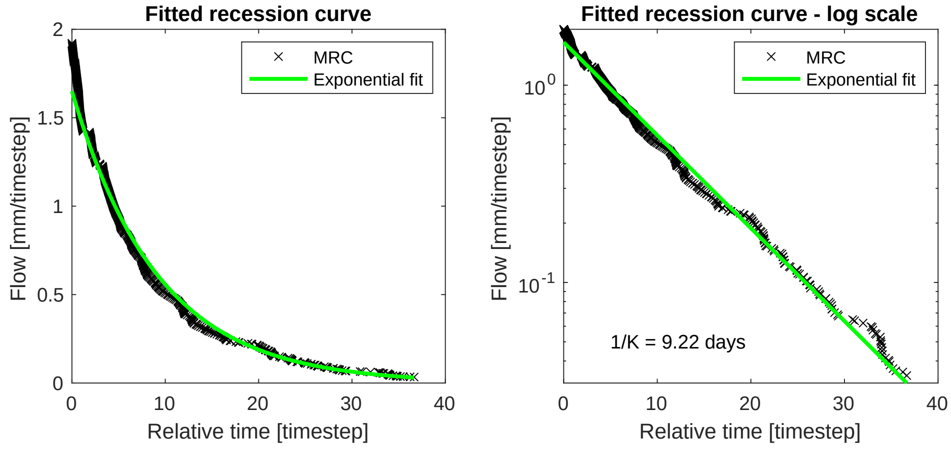

Fig. D6 Master recession curve (MRC) for the Flatlick Branch catchment.

mobilization levels, which range from a Mobilization Level 1 (corresponding to a recommended daily road salt application to impervious surfaces of 0.025 kg m^{-2}) to Mobilization Level 5 (corresponding to a recommended road salt application of 0.048 kg m^{-2}) (Table E2). The mobilization levels, in turn, depend on forecasts of precipitation probability, snow accumulation depth and ambient temperature (Table E2, see also Appendix D.a in Moltz et al. [64]). We re-constructed a ten-year timeseries of daily mobilization levels at Flatlick Branch based on historical weather data recorded at Dulles Airport (i.e., we used actual historical weather data as a proxy for historical weather forecasts, which were not available for the ten year period of interest here). To evaluate how well these simulated mobilization levels comport with reality, we obtained from VDOT the actual daily mobilization levels recorded for the Northern Virginia region during the winter seasons of 2019 and 2020. Mobilization levels predicted with measured climate data at Dulles (black bars Figure E7) compare favorably with actual mobilization levels recorded by VDOT (red bars Figure E7), although there are many cases where the actual mobilization level was higher than the predicted mobilization level, and more infrequently cases where the actual mobilization level was lower than the predicted mobilization level. These differences are due to weather forecast inaccuracies (e.g., that might predict precipitation when no precipitation in fact occurred) and the fact that the conditions listed for each mobilization level in Table E2 are just recommended guidelines; other factors, such as profession judgement [65], often influence the mobilization levels adopted on any particular winter day (personal communication, VDOT staff).

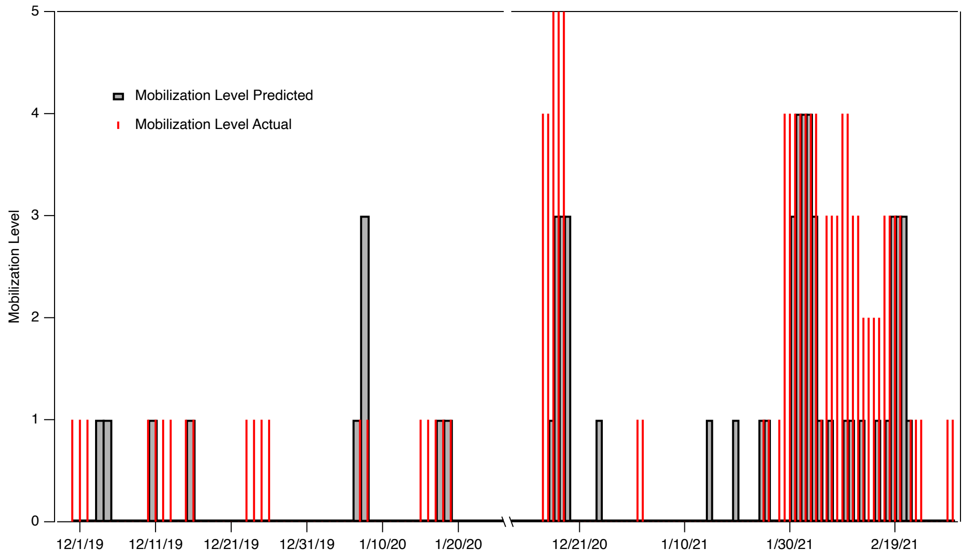

Fig. E7 Comparison of actual and model predicted winter weather mobilization levels in Northern Virginia for a two-year period.

Table E2 Salt Institute's standard road salt (as NaCl) application rates

Weather Forecast	Winter-Weather Mobilization Level	Road Salt (NaCl) Application Rate (kg/m^2)
P: >20%; S: possible; T: 30-36	Anti-ice	0.025
P: 20-49%; S: possible; T: 30-36	1	0.025
P: 50-100%; S: $<$ 1 inch; T: 25-29	2	0.031
P: 50-100%; S: $<$ 2 inch; T: 20-24	3	0.037
P: 50-100%; S: $<$ 6 inch; T: 15-19	4	0.042
P: 50-100%; S: $>$ 6 inch; T: 10-14	5	0.047

P: Chance of precipitation; S: Snowfall; T: Temperature (°F).

Appendix F Inferring Chloride Concentrations from Specific Conductance

To contextualize the specific conductance (SC) measurements on Flatlick Branch, we estimated from the SC measurements stream chloride concentrations which can, in turn, be directly compared to the U.S. Environmental Protection Agency's 1988 Ambient Water Quality Criteria for stream chloride concentration (chronic and acute thresholds of 230 and 860 mg L^{-1}, respectively) (EPA 1988). To convert SC measurements into chloride concentrations we utilized USGS measurements of SC and chloride on 27 grab samples collected at our field site on a monthly basis for the past three calendar years (2020-2022). Regressing log-transformed chloride against log-transformed

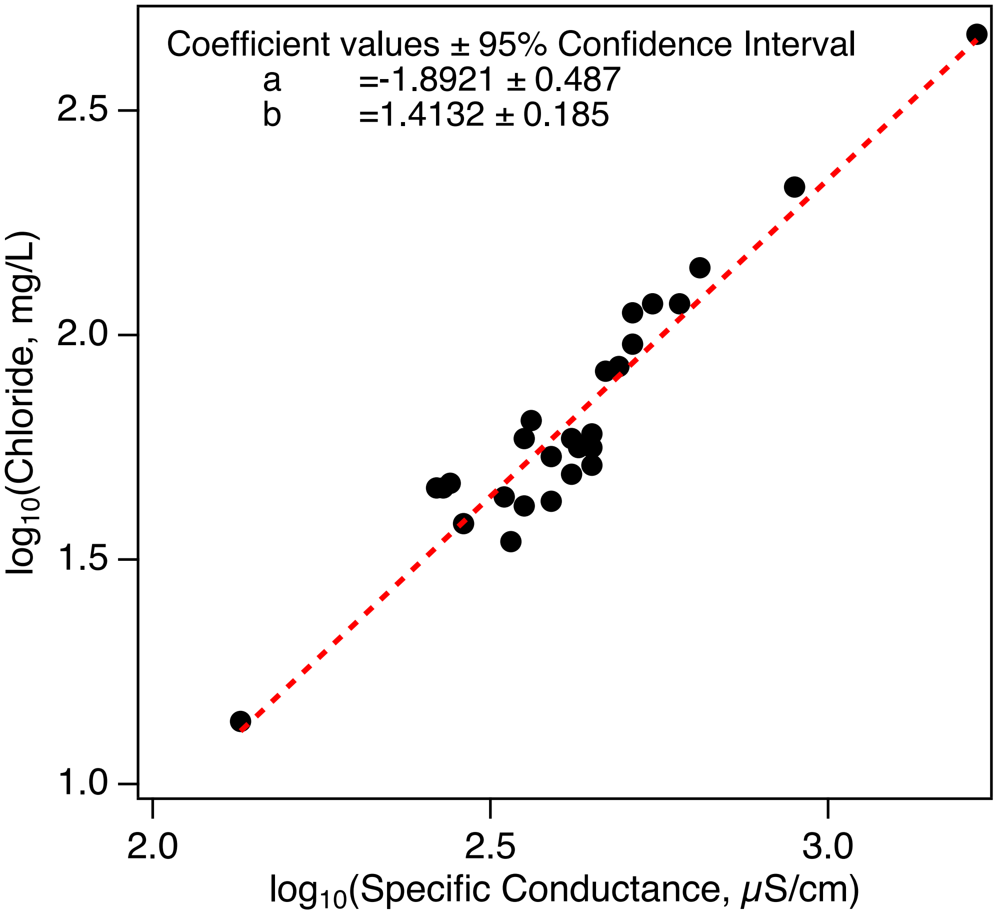

Fig. F8 Measured chloride vs in-stream specific conductance at Flatlick Branch.

SC we obtain the following power-law relationship between the two: $[\mathrm{Cl}] = 10^a \times \mathrm{SC}^b$, where $a = -1.89 \pm 0.48$ and $b = 1.41 \pm 0.18$ (R^2=0.91) (Figure F8).

Appendix G Deicer Application Rates and Stream Salinity

Analysis of salinity measurements on Flatlick Branch reveals a cause-and-effect relationship between peak stream salinity and rough estimates for the cumulative area-normalized mass of road salt deposited in the lead up to a snow melt event (Figure G9). The latter was estimated by first generating a daily time series of recommended salt application (in units of kg m^{-2}) based on local deicer application guidelines [64] and historical weather data (Section E). Over the eight year calibration and validation periods, we then summed the predicted daily mass of road salt (as sodium chloride)

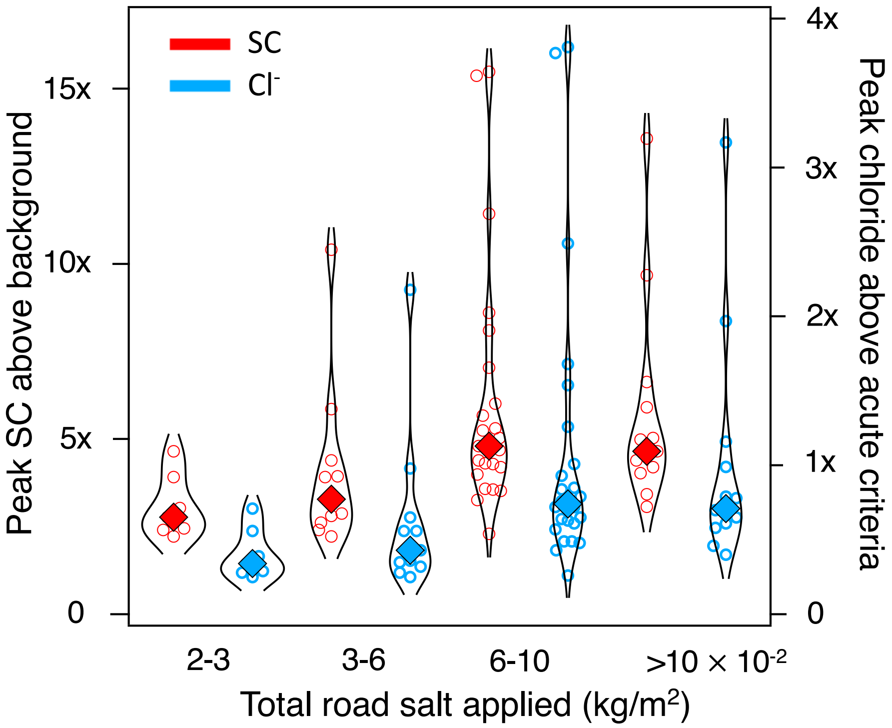

Fig. G9 Cause-and-effect relationship at Flatlick Branch between the cumulative road salt applied in the lead-up to a storm, and the peak stream SC and inferred chloride concentrations during snow melt events.

applied from the end of the penultimate storm to the snow melt event in question. Measurements of peak stream salinity at Flatlick Branch increase non-linearly with these predictions of cumulative deicer application, from at least two times the background level for 0.02 to 0.03 kg NaCl m^{-2} to between three and fifteen times the background level for > 0.1 kg NaCl m^{-2} (red symbols in Figure G9). These specific conductance values can be roughly translated into chloride concentrations using the site-specific regression relationship described in Section F. At higher salt application rates the inferred peak stream chloride concentrations are nearly four times the U.S. EPA acute aquatic life threshold of 860 mg L^{-1} (blue symbols in Figure G9).

Appendix H Groundwater Specific Conductance in the Mesozoic Lowland HGMR

We compiled historical data [42, 81] and data available thorough the National Groundwater Monitoring Network (cida.usgs.gov/ngwmn), on specific conductance measured in groundwater wells (depths ranging from 80-1000 feet) in the Mesozoic Lowland hydrogeomorphic (HGMR) region of Virginia. Measured specific conductance in deep groundwater ranged from 62-4500 uS/cm, with a median value of 542.5 uS/cm (Figure 3). These data are compiled in Tables H3-H5.

Table H3 Groundwater Specific Conductance for Wells in the Mesozoic Lowland HGMR Reported in Posner and Zenome, 1983

USGS Local Reference No.	Date	Depth of Well (feet)	Specific Conductance (uS/cm)
EC-10	11/27/79	858	970
51V-3E	7/30/75	100	780
51V-3E	7/30/75	520	750
51V-3E	7/30/75	900	4500
51V-24H	7/20/79	500	560
51V-24H	7/26/79	760	2000
50U-83C	6/24/80	-	2140
50U-84F	6/24/80	-	644
50T-16B	7/30/80	153	433
50S-2D	5/02/80	205	439
48R-3A	6/17/80	-	2710
DC-31	10/18/78	285	355
DB-47	10/18/78	600	275
51V-14F	10/24/78	423	295
51V-14F	10/25/88	880	290
51V-23H	7/09/79	1000	640
51V-5J	1/13/77	289	150
49U-11C	4/28/80	500	254
48R-4A	6/17/80	100	414
47R-11G	8/12/80	-	412

Appendix I Deconvolution Framework

As noted above, the T-TTD model produces time-varying estimates for the age-distribution of water in the stream, $p_{\text{stream}}(T,t)$ (units inverse age) where T is water age and t is time (units of age and time, respectively). The increment of salt mass discharged from the stream per unit time with age in the range T to $T+\Delta T$ at time t is therefore $\Delta\dot{M}_Q(T,t) = \dot{M}_Q(t)p_{\text{stream}}(T,t)\Delta T$. Here $\dot{M}_Q(t)$ (units of salt mass per time) is the measured salt mass discharged from the stream at time t (equal to measured salt concentration times measured stream discharge) and $\Delta\dot{M}_Q(T,t)$ is the portion of that discharged salt mass with age T at time t. The rate at which salt was added to the catchment (e.g., as deicers) at "injection" time $\tau = t - T$ is therefore the sum over all $\Delta\dot{M}_Q(T,t)$ for which the difference of t and T equals τ:

$$\dot{M}_J(\tau) = \sum_{\tau=t-T} \Delta\dot{M}_Q(T,t) \qquad \text{(I13)}$$

This can be visualized graphically by imagining a matrix in which the rows and columns represents time t and stream water age T, respectively, and the entries are our estimate of $\Delta\dot{M}_Q(T,t)$ obtained from the measured stream salt mass loading rate

Table H4 Groundwater Specific Conductance for Wells in the Mesozoic Lowland HGMR Reported in Froelich and Zenome, 1985

USGS Local Reference No.	Date	Depth of Well (feet)	Specific Conductance (uS/cm)
385320077251701	7/05/79	743	931
385320077251701	7/09/79	1000	538
384810077284501	4/18/77	320	600
384918077281201	4/17/77	290	437
385321077234001	12/21/76	309	160
385311077234501	1/13/77	289	150
385157077275301	4/20/77	400	398
385543077271901	8/18/75	860	1170
385617077271201	7/30/75	100	780
385617077271201	7/30/75	530	750
385617077271201	7/30/75	900	4500
385048077320001	4/20/77	-	585
385656077241201	10/04/74	-	215
390130077210801	10/04/74	-	320
390109077210701	10/04/74	-	188
385657077232701	11/12/74	-	200
385350077272501	7/20/79	500	547
385350077272501	7/26/79	500	2050
385205077275501	6/20/79	650	570
385205077275501	8/09/76	650	849

Table H5 Groundwater Specific Conductance for Wells in the Mesozoic Lowland HGMR in Virginia from the National Groundwater Monitoring Network (cida.usgs.gov/ngwmn)

USGS Local Reference No.	Date	Depth of Well (feet)	Specific Conductance (uS/cm)
385930000000000	7/22/03	120	551
385930000000000	7/22/03	120	507
385930000000000	2/03/05	120	330
385930000000000	2/03/05	120	432
385930000000000	5/05/05	120	482
385930000000000	5/05/05	120	445
385930000000000	8/01/05	120	520
385930000000000	8/01/05	120	523
385930000000000	8/07/07	120	599
385930000000000	8/07/07	120	606
385930000000000	7/28/09	120	698
385930000000000	7/28/09	120	712
385930000000000	8/17/11	120	795
385930000000000	8/17/11	120	784
385930000000000	8/12/15	120	977
385930000000000	8/12/15	120	946
384956000000000	7/23/03	80	62
384956000000000	7/23/03	80	66
384956000000000	7/28/15	80	72
384956000000000	7/28/15	80	74

and our T-TTD theory estimates for the age distribution, $p_{\mathrm{stream}}(T,t)$ (see above). The salt mass loading rate to the catchment at time τ is simply the sum over all cells in the matrix that fall along the line, $t = \tau + T$ [82, 83].

Appendix J Additional Supplementary Figures

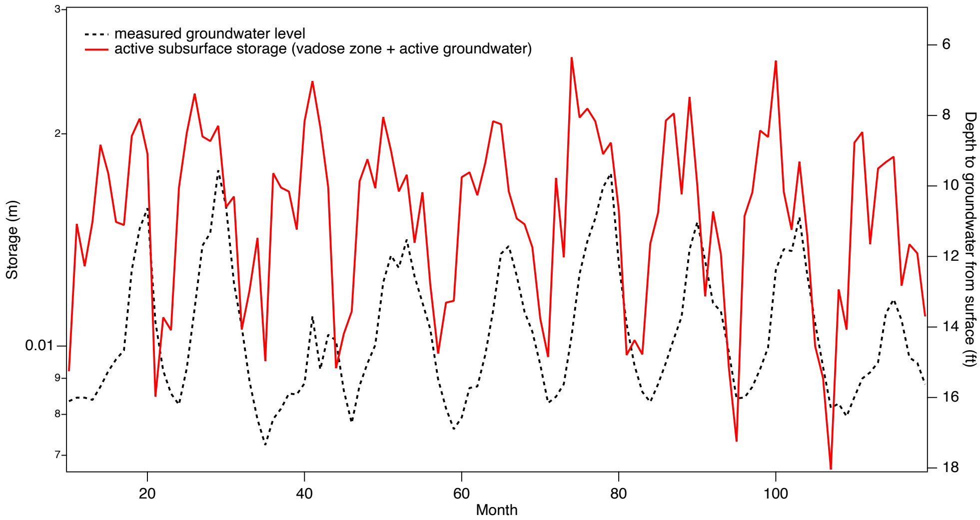

Fig. J10 Model-predicted storage (monthly averaged) in the vadose zone and groundwater (red curve) follows a seasonal pattern similar to that of the monthly groundwater level observed at a nearby USGS monitoring well (USGS well #385638077220101, see Figure A1)

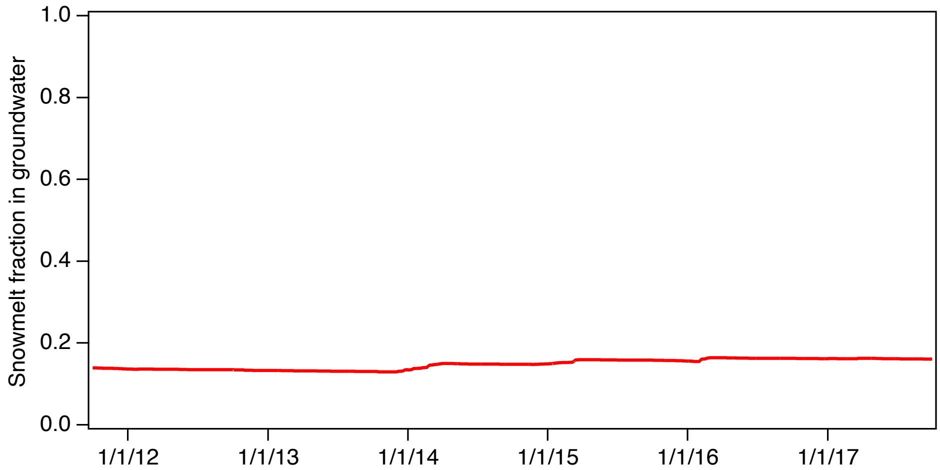

Fig. J11 Model-predicted fraction of snow melt in groundwater for the validation period.

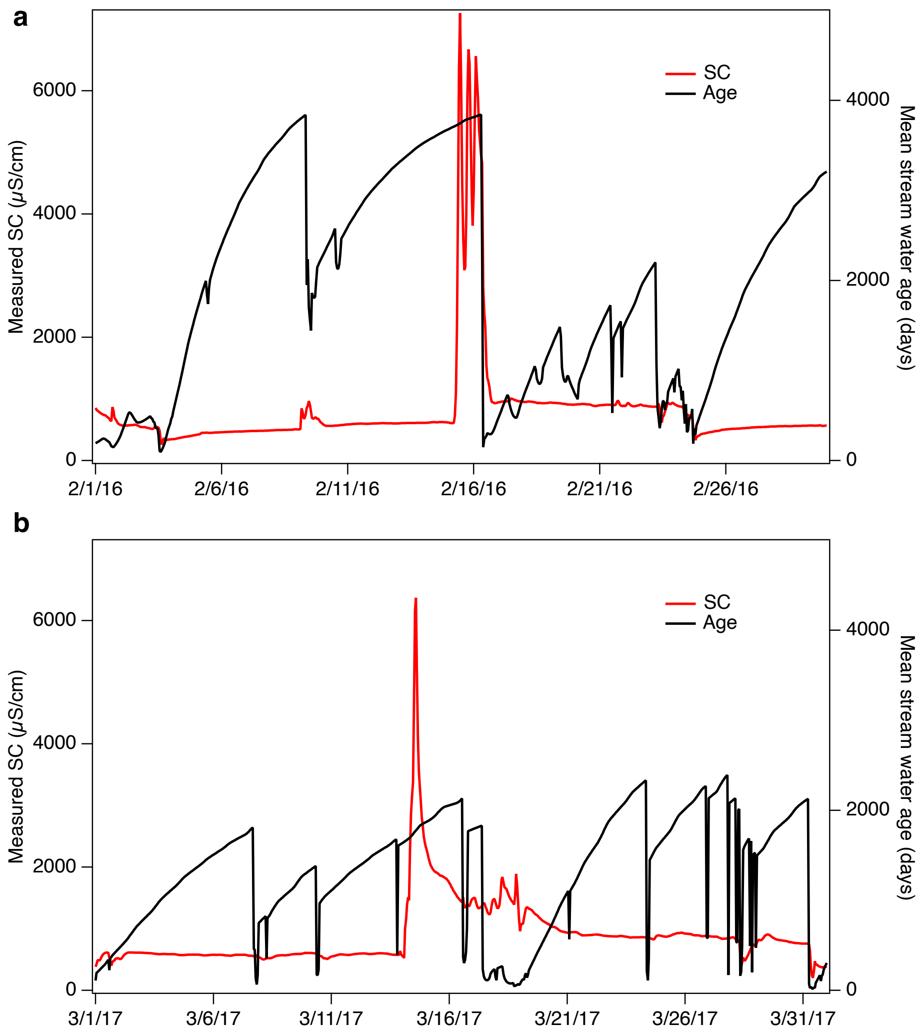

Fig. J12 Illustrative examples of periods when peaks in measured stream specific conductance (SC) do not perfectly align with reductions in the mean stream water age (reflecting contribution from younger direct runoff and/or interflow). SC pulses either arrive early (panel a) or are delayed (panel b) with respect to younger flows from direct runoff and/or interflow.